International Journal of Applied Earth Observation and Geoinformation 118 (2023) 103297

Contents lists available at ScienceDirect

International Journal of Applied Earth Observation and Geoinformation

journal homepage: www.elsevier.com/locate/jag

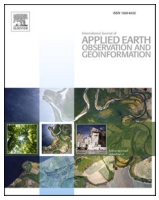

Most complicated lock pattern-based seismological signal framework for automated earthquake detection

Suat Gokhan Ozkaya [a], Nursena Baygin [b], Prabal D. Barua [c,d,e,f,g,h,i,j,k], Arvind R. Singh [l,*], Mohit Bajaj [m,s], Mehmet Baygin [n], Sengul Dogan [o], Turker Tuncer [o], Ru-San Tan [p,q], U. Rajendra Acharya [r]

[a] Department of Construction Technologies, Technical Sciences Vocational School, Ardahan University, Ardahan, Turkey
[b] Department of Computer Engineering, Faculty of Engineering, Erzurum Technical University, Erzurum, Turkey
[c] Cogninet Australia, Sydney, NSW 2010, Australia
[d] School of Business (Information System), University of Southern Queensland, Australia
[e] Faculty of Engineering and Information Technology, University of Technology Sydney, Sydney, NSW 2007, Australia
[f] Australian International Institute of Higher Education, Sydney, NSW 2000, Australia
[g] School of Science &, Technology, University of New England, Australia
[h] School of Biosciences, Taylor's University, Malaysia
[i] School of Computing, SRM Institute of Science and Technology, India
[j] School of Science and Technology, Kumamoto University, Japan
[k] Sydney School of Education and Social Work, University of Sydney, Australia
[l] Department of Electrical, Electronic and Computer Engineering, University of Pretoria, South Africa
[m] Department of Electrical Engineering, Graphic Era (Deemed to be University), Dehradun 248002, India
[n] Department of Computer Engineering, Faculty of Engineering, Ardahan University, Ardahan Turkey
[o] Department of Digital Forensics Engineering, College of Technology, Firat University, Elazig Turkey
[p] Department of Cardiology, National Heart Centre Singapore, Singapore
[q] Duke-NUS Medical School, Singapore
[r] School of Mathematics, Physics and Computing, University of Southern Queensland, Springfield, Australia
[s] Applied Science Research Center, Applied Science Private University, Amman-11931, Jordan

ARTICLE INFO

Keywords:
MCLP
Earthquake prediction
Explainable feature engineering
Seismological signal processing
XAI

ABSTRACT

Background: Seismic signals record earthquakes and also noise from different sources. The influence of noise makes it difficult to interpret seismograph signals correctly. This study aims to develop a computationally lightweight, accurate, and explainable machine learning model for the automated detection of seismogram signals that could serve as an effective warning system for earthquake prediction.

Material and method: We developed a handcrafted model for earthquake detection using a balanced dataset of 5001 earthquakes and 5001 non-earthquake signal samples. The model included multilevel feature extraction, selector-based feature selection, classification, and post-processing. Input signals were decomposed using tunable Q wave transform and fed to a statistical and textural feature extractor based on the most complicated lock pattern (MCLP). Four feature selectors were used to choose the most valuable features for the support vector machine classifier. Additionally, voted vectors were generated using iterative hard majority voting. Finally, the best model was chosen using a greedy algorithm.

Results: The presented self-organized MCLP-based feature engineering model yielded 96.82% classification accuracy with 10-fold cross-validation using the seismic signal dataset.

Conclusions: Our model attained high seismological signal detection performance comparable with more computationally expensive deep learning models. Our handcrafted explainable feature engineering model is computationally less expensive and can be easily implemented. Furthermore, we have introduced a competitive feature engineering model to the deep learning models for the seismic signal classification model.

* Corresponding author.
E-mail addresses: suatgokhanozkaya@ardahan.edu.tr (S. Gokhan Ozkaya), nursena.baygin@erzurum.edu.tr (N. Baygin), Prabal.Barua@usq.edu.au (P.D. Barua), u17410411@tuks.co.za (A.R. Singh), thebestbajaj@gmail.com (M. Bajaj), mehmetbaygin@ardahan.edu.tr (M. Baygin), sdogan@firat.edu.tr (S. Dogan), turkertuncer@firat.edu.tr (T. Tuncer), tan.ru.san@singhealth.com.sg (R.-S. Tan), Rajendra.Acharya@usq.edu.au (U. Rajendra Acharya).

https://doi.org/10.1016/j.jag.2023.103297
Received 12 February 2023; Received in revised form 17 March 2023; Accepted 5 April 2023
Available online 14 April 2023

1. Introduction

An earthquake is the result of geological movements of the Earth's tectonic plates, which induce a sudden release of energy through to its crust (Bolton, Shreedharan, Rivière, & Marone, 2020; Wald, 2020). This generates seismic waves that spread across the Earth's surface; the two main types being P and S waves (Saraf, Rawat, Choudhury, Dasgupta, & Das, 2009). While the waves' point of origin localizes the earthquake's source, its intensity is determined by the area extent of underground shaking that eventually breaches the ground surface (An, Tao, Jiang, & Yan, 2021; Z. Li, Meier, Hauksson, Zhan, & Andrews, 2018), as well as earthquake depth (Eftekhari, Samadzadegan, & Javan, 2023), defined as the distance between the point of energy origin and its arrival at the Earth's surface (Rost, Earle, Shearer, Frost, & Selby, 2015). The environmental impact of an earthquake can be qualitatively assessed using the widely known Richter scale (Pavel, 2021)–a scale of 8 or greater denotes a destructive earthquake–while the magnitude of the mechanical effect can be more precisely quantified using seismographs, which can detect earthquakes of scale 2.5 or less that are otherwise usually not felt (van der Meijde, Pail, Bingham, & Floberghagen, 2015).

Seismographs continuously record the magnitude, duration, timing and center of ground seismic waves (Wang, DeGrandpre, Lu, & Freymueller, 2018), and may be used in early warning systems to forecast major earthquakes (Bolton et al., 2020). However, there are some limitations (Wald, 2020). Other than earthquakes, seismic waves can be generated by environmental events as well as human activities (Z. Li et al., 2018), e.g., volcanic eruptions, underground chemical explosions, helicopters, trains, traffic, etc. (Mandal & Maiti, 2015). These non-earthquake seismic signals are also captured on seismograms, which causes significant data pollution, rendering it difficult to analyze ground activity for earthquake prediction. For effective prediction, earthquake and non-earthquake signals must be separated timeously, which can be demanding with manual methods (Malfante et al., 2018). Artificial intelligence-enabled automatic signal classification, which has been actively applied in many fields, e.g., healthcare (Tasci et al., 2023), offers a potential solution for the efficient analysis of dense seismogram signals. In this paper, we report a novel machine learning-based model for automated binary classification of seismogram signals into earthquake versus non-earthquake signal categories, which has attained > 96% classification accuracy when trained on a public three-channel seismogram dataset (Magrini, Jozinović, Cammarano, Michelini, & Boschi, 2020).

1.1. Literature review

We performed a nonsystematic review of recent publications of machine learning approaches for the automated classification of seismographic data (Table 1). Most of the methods are based on deep learning, which can be computationally complex and expensive. Even so, many deep models attained only modest classification accuracy. Further, none of these models used explainable artificial intelligence (XAI), which can potentially garner wider acceptance by improving model interpretability (Loh et al., 2022).

1.2. Motivation and our model

We aimed to develop a computationally lightweight, accurate, and explainable machine learning model for the automated classification of seismogram signals that could serve as an effective warning system for earthquake prediction. Generally, machine learning-based systems can efficiently use data to solve nondeterministic polynomial problems, but only by incorporating XAI can the user be better equipped to understand how the model learns from the data. For this work, we used a seismogram dataset comprising three channels (X, Y, and Z) and have developed a handcrafted explainable feature engineering (XFE) model for earthquake detection using seismogram signals that could explain the individual as well as combined channel effects for earthquake prediction. Handcrafted feature generators focus on improving model performance by capturing relevant information, while handcrafted XFE is employed toexplain the model's predictions. In other words,

Table 1
Summary of machine learning methods for earthquake detection.

Paper	Method	Dataset	Key points and limitations
Otovic et al., 2022 (Otović et al., 2022)	Custom-designed convolutional neural network (CNN) (ConvNetQuake)	Len-DB (Magrini et al., 2020)	Earthquake magnitude determination; 86:14 holdout validation; high time complexity; relatively low accuracy
Magrini et al., 2020 (Magrini et al., 2020)	Custom designed CNN	Len-DB (Magrini et al., 2020)	Earthquake/noise detection; 71:21.5:7.5 holdout validation; 96.7% (training), 95.3% (validation), 93.2% (test) accuracies; high time complexity
Majstorović et al., 2021 **(Majstorović, Giffard-Roisin, & Poli, 2021)**	Custom designed CNN	Own dataset	Earthquake/noise detection (stage 1) and earthquake characterization (stage 2); 80:10:10 holdout validation; 97% (stage 1) and 68% (stage 2) accuracies; high time complexity
Kong et al., 2021 (Kong et al., 2021)	Autoencoder-based feature extraction; CNN	Len-DB (Magrini et al., 2020)	Earthquake/noise detection; >90% accuracy; high time complexity
Mousavi and Beroza, 2019 (Mousavi & Beroza, 2020)	CNN; long short term memory	STEAD (Mousavi, Sheng, Zhu, & Beroza, 2019)	Earthquake magnitude determination; 70:10:20 holdout validation; high time complexity
Zhu et al., 2022 (Zhu, Tai, Mousavi, Bailis, & Beroza, 2022)	Custom-designed CNN (EQNet)	STEAD (Mousavi et al., 2019)	P and S picking determination and earthquake time detection; cross-validation strategy; good P and S wave arrival detection; high time complexity
Saad et al., 2022 (Saad et al., 2022)	Short-time frequency transform; unsupervised deep learning; attention networks	STEAD (Mousavi et al., 2019)	Data denoising process on single-channel earthquake data; signal-to-noise ratio 1.95 dB; high time complexity; threshold difficulty in obtaining the appropriate binary mask
Li et al., 2022 (**W.** Li et al., 2022)	Custom-designed CNN based on residual network (1D ResNet34)	SCEDC (Hafner & Clayton, 2001)	P wave, S wave and noise classification; 50:25:25 holdout validation; 98.70% accuracy; high time complexity
Jozinović et al. (Jozinović, Lomax, Štajduhar, & Michelini, 2020)	Custom designed CNN	Own dataset	Earthquake/noise detection; high-time complexity
Kavianpour et al. (Kavianpour, Kavianpour, Jahani, & Ramezani, 2021)	CNN, Bi-directional long-short-term memory	Own dataset	Earthquake magnitude prediction, 80:20, RMSE: 0.0982, high time complexity
Meier et al. (Meier et al., 2019)	Custom-designed CNN, a generative adversarial network	SCSN data	Precision: 99.50, recall: 99.30, Accuracy: 99.50

CNN, convolutional neural network; Len-DB, Local Earthquakes and Noise DataBas; SCEDC, The Southern California Earthquake Data Center; STEAD, STanford EArthquake Dataset; SCSN, Southern California Seismic Network.

handcrafted XFE is a subset of handcrafted feature generation, requiring the features to be interpretable and explainable. In this context, our framework comprised the following components: hybrid multilevel feature extraction based on tunable Q wave transform (TQWT) signal decomposition (Selesnick, 2011) combined with statistical and–using a novel most complicated lock pattern (MCLP)–textural feature extraction; feature selection using multiple feature selectors; classification using support vector machine (SVM) (Vapnik, 1998); and post-processing to obtain best-voted results using iterative hard majority voting (IHMV) (Dogan et al., 2021).

1.3. Theoretical background

Deep learning models for analyzing seismographic data have exponential computational complexity (Ghanbari & Antoniades, 2022; Lv, Chen, Dou, & Plaza, 2022; Qing et al., 2022; Xiu et al., 2023); feature engineering models generally possess linear complexity and are computationally more efficient and less costly (Wei et al., 2022). However, handcrafted feature generators cannot extract features at high levels for accurate prediction. To resolve this, multilevel deep feature extraction can be simulated using signal decomposition techniques to transform the seismogram signal into wavelet bands and input the decomposed wavelet band (plus raw seismogram signal) into downstream feature extractors, where both statistical and textural features can be extracted in parallel. The former involves the calculation of standard statistical moments from the input signals. For the latter, we were inspired by the popular MCLP–one of the best-submitted solutions for the Summer of Math Exposition (Zye, 2021) –to build a novel textural feature extractor using MCLP-generated directed graphs. The basic premise of MCLP involves finding the most complicated path for unlocking an Android mobile phone (as determined by preset rules) that joins all the 3×3 dots on the opening screen; the problem is generalizable to larger square or even rectangular dot matrixes (Zye, 2021). In this work, we used a MCLP based on a 3×3 dot matrix and a statistical feature generator to extract multiple textural and statistical features, respectively, from each input seismogram signal and its TQWT-decomposed wavelet bands. To reduce redundant features, four different feature selectors, each with its own unique attributes, were deployed downstream to select the most discriminative feature vectors. These were fed to a standard shallow SVM classifier for calculating prediction vectors, which were post-processed using IHMV to generate the best-voted prediction vectors. Finally, the relative contributions of the different seismic signal channels, either individually or in combination, and feature selectors toward model performance were mapped out, yielding insights into the most valuable input signals and model components, enhancing model interpretability and potentially facilitates model optimization.

1.4. Innovations and contributions

Innovations (novelties) and contributions of this research are clarified below.

Innovation:

- MCLP is an information security theorem. We have used this pattern to generate a new generation feature creation function.
- A novel self-organized XFE model has been introduced using the recommended MCLP feature extractor, TQWT (it has been used to generated features at frequency domain), four feature selector, SVM and IHMV.

Contributions:

- Proposed a novel MCLP-based feature engineering method combining signal decomposition, statistical feature extraction, multiple feature selectors, SVM, IHMV, and XFE with building a parametric network for self-organized automated classification of seismic signals. Our model analyzed seismic signals channel-wise and presented the most valuable channel for this problem. Furthermore, we have explained the most informative features, bands, feature selection function and SVM kernel for solving this seismic signal classification problem.
- Our presented MCLP-based XFE attained is a lightweight (computationally efficient) classification model.
- Attained higher performance than the state-of-the-art techniques developed for discriminating earthquake seismic signals.

1.5. Organization

The rest of the study is organized as follows. Section 2 describes the data used and methods employed. Section 3 reports the results obtained using the developed model. The obtained results are discussed in Section 4, and also the results are compared with the other reported results using similar datasets. Also, the highlights and limitations of the developed model are presented in this section. Finally, conclusions are given in Section 5.

2. Materials and methods

2.1. Dataset

From a public dataset (Magrini et al., 2020) containing three-channel (X, Y and Z) seismogram signals, each of length 27 s with sampling frequency 20 Hz, i.e., data length 540 ($=27 \times 20$). We built a balanced dataset with $>$ 10,000 observations by selecting the first 5001 earthquakes and the first 5001 non-earthquake seismogram signals (Fig. 1).

2.2. Proposed model

Our handcrafted model comprising four phases–multilevel feature extraction, multiple selector-based feature selection, classification, and post-processing (Fig. 2) –possessed linear time complexity and is thus less computationally demanding than deep learning models. The individual channel-wise seismogram signals–X, Y, and Z–and a concatenated signal obtained by merging all three channel signals were input into the model. First, each input signal would undergo TQWT decomposition into eight wavelet bands. The latter and the raw input signal would be fed to statistical and MCLP-based textural feature extractor functions to generate four feature vectors, which were merged to obtain a fifth feature vector. All five feature vectors were fed to four feature selectors–neighborhood component analysis (NCA) (Goldberger, Hinton, Roweis, & Salakhutdinov, 2004), ReliefF (Robnik-Šikonja & Kononenko, 2003), minimum redundancy maximum relevance (mRMR) (Radovic, Ghalwash, Filipovic, & Obradovic, 2017), and Chi2 (Liu & Setiono, 1995)–to generate a total of 20 ($=5 \times 4$) selected feature vectors containing the most valuable features, which were fed to a standard shallow SVM classifier to calculate the respective 20 predicted vectors. The latter were post-processed using IHMV (Dogan et al., 2021) to generate an additional 18 voted vectors. From the 38 combined predicted and voted vectors, a greedy algorithm was applied to select the most accurate final result. Details of each phase are explained in the following subsections.

2.2.1. Signal decomposition

In this paper, the TQWT method is used for signal decomposition. TQWT (Selesnick, 2011) is a decomposition method frequently used in the literature on signal processing. TQWT is a bandwidth-adjustable approach that can analyze over multiple scales and frequency ranges. This method separates features in a specific frequency range and identifies similarities or differences between signals. In addition, the tunable

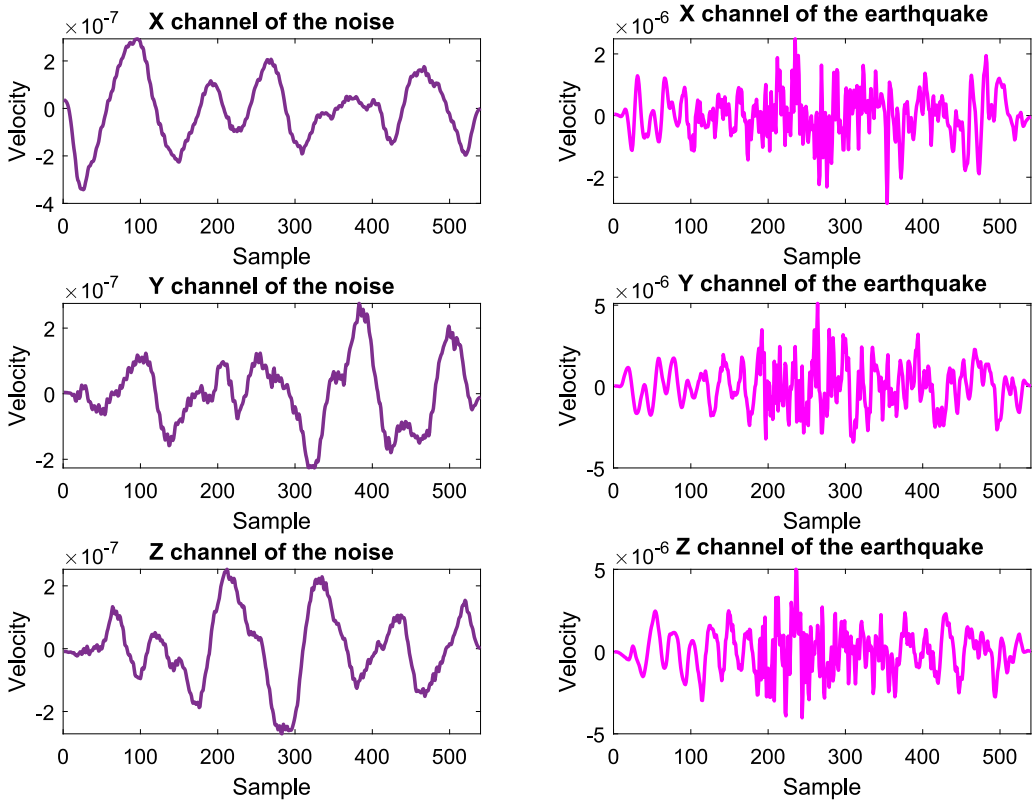

Fig. 1. Examples of non-earthquake (noise) and earthquake seismograms belonging to the three signal channels.

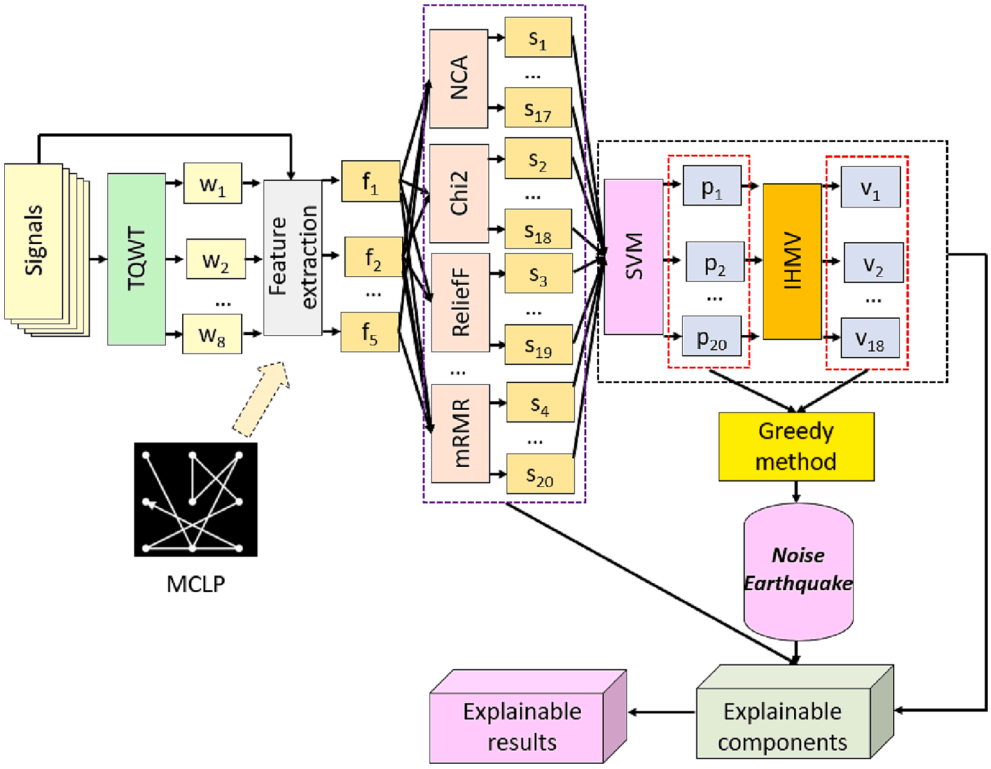

Fig. 2. Schema of the proposed explainable feature engineering model. **f, feature vector; p, predicted vector; s: selected feature vector; v, voted vector; w, wavelet band.

nature of TQWT decomposes the signals into different frequency components.

The TQWT method uses wavelet oscillations (Q), reduction coefficient (r), and the number of levels (J) tuning parameters to obtain multilevel wavelet transforms. In this study, eight wavelet bands were obtained using the TQWT method. Various features were extracted from these sub-bands.

2.2.2. Feature extraction

The input seismogram signal (i.e., Channel X, Y, or Z, or concatenated signal of all three channels) was decomposed using TQWT to generate eight wavelet bands. These, decomposed signals with raw signals were fed to statistical and MCLP-based textural feature extractors. The former calculated 14 statistical moments (minimum, maximum, average, median, standard deviation, mean absolute deviation, energy, wavelet entropy, information entropy, Tsallis entropy, sure entropy, Renyi entropy, log entropy, and threshold entropy), generating 14 statistical features (Kuncan, Yılmaz, & Kuncan, 2019). MCLP, a new local binary pattern-like textural feature extractor, created another 256 features. Accordingly, 270 features were extracted in total for every one of the eight decomposed wavelet bands or raw input, i.e., the length of each of the four feature vectors corresponding to Channel X, Y, Z and the concatenated signal was 2430 (= (256 + 14) × (8 + 1)). Finally, the four vectors were concatenated to form a fifth feature vector of length 9720 (=2430 × 4) (Fig. 3).

The steps involved in feature extraction are detailed below.

Step 1: Create four signals from the channel-wise seismogram signals and the concatenated signal resulting from merging all three channels.

$$c^1(j) = signal(j,1), j \in \{1,2,\cdots,L\}$$

$$c^2(j) = signal(j,2)$$

$$c^3(j) = signal(j,3)$$

$$c^4(j+L\times(t-1)) = signal(j,t), t \in \{1,2,3\} \quad (1)$$

where c^1, c^2, c^3 and c^4 represent channel ×, channel y, channel z and the merged channel signal, respectively; and L, the length of each channel.

Step 2: Apply TQWT to each signal to calculate wavelet bands.

$$w_i^k = \tau\left(c^k, 1, 3, 7\right), k \in \{1,2,3,4\}, i \in \{1,2,\cdots,8\} \quad (2)$$

where w represents the wavelet band; and τ, TQWT.

Step 3: Extract features by deploying signals, wavelet bands, and the used feature extractors.

$$x_1^k = \varpi\left(\zeta\left(c^k\right), \psi\left(c^k\right)\right), k \in \{1,2,3\}$$

$$x_{i+1}^k = \varpi\left(\zeta\left(w_i^k\right), \psi\left(w_i^k\right)\right), i \in \{1,2,\cdots,8\}$$

$$f^k = \varpi\left(x_1^k, x_2^k, \cdots, x_9^k\right) \quad (3)$$

where x represents extracted features (with the length of 270 (=256 + 14)); $\varpi(.)$, merging function; $\zeta(.)$, statistical feature generator (the 14 calculated moments are listed above); and $\psi(.)$, MCLP function used for textural feature extraction (Fig. 4).

The steps involved in MCLP-based textural feature extraction are detailed below.

Step 3.1: Load the signal.

Step 3.2: Create an overlapping block of length 9.

Step 3.3: Apply vector2matrix transformation to each overlapping block to create 3 × 3 matrixes, on which the MCLP is applied.

Step 3.4: Apply the MCLP-directed graph (Fig. 5) for textural feature extraction.

Using signum function as a binary feature extraction kernel, eight bits were extracted sequentially according to the eight numbered directed edges (Fig. 5), as defined below.

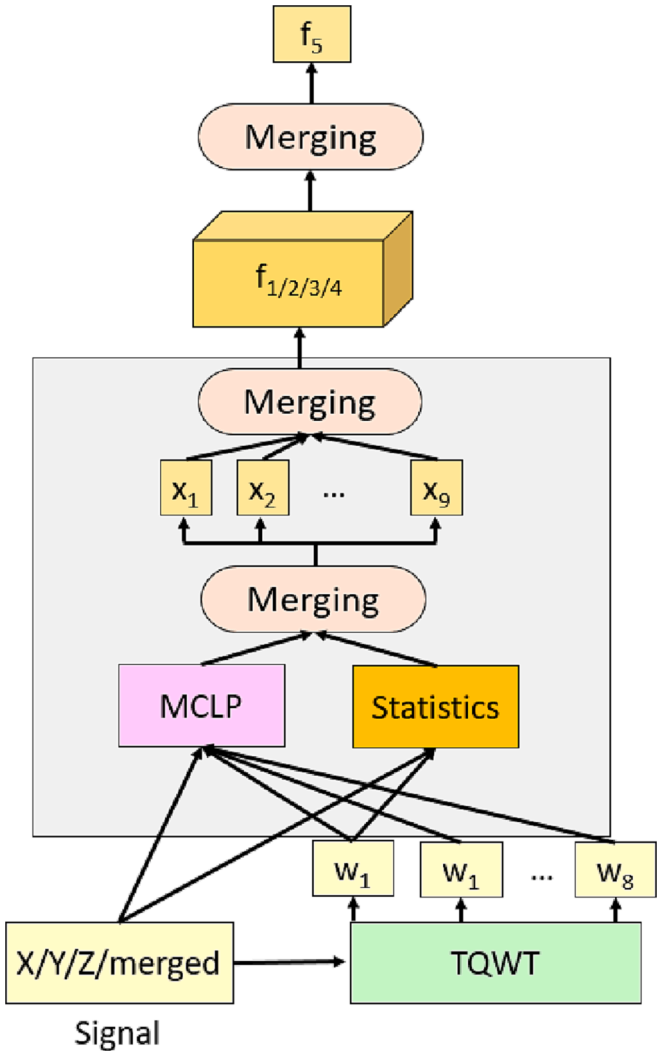

Fig. 3. Schema of the feature extraction method. **f, feature vector; w, wavelet band; x, merged textural and statistical features extracted from raw seismogram or individual wavelet band.

$$\begin{vmatrix} b_1 \\ b_2 \\ b_3 \\ b_4 \\ b_5 \\ b_6 \\ b_7 \\ b_8 \end{vmatrix} = \delta\left(\begin{vmatrix} m_{1,1}, m_{3,2} \\ m_{3,2}, m_{1,3} \\ m_{1,3}, m_{2,2} \\ m_{2,2}, m_{1,2} \\ m_{1,2}, m_{2,3} \\ m_{2,3}, m_{3,1} \\ m_{3,1}, m_{3,3} \\ m_{3,3}, m_{2,1} \end{vmatrix}\right) \quad (4)$$

$$\delta(x,y) = \begin{cases} 0, x-y<0 \\ 1, x-y \geq 0 \end{cases} \quad (5)$$

where $\delta(.)$ represents the signum function, which takes two parameters (x,y); m, the matrix of size 3 × 3; and b, generated bits. In the MCLP transformation, 8 bits were extracted per signal block.

Step 3.5: Generate map signal.

$$map(h) = \sum_{i=1}^{8} b_i \times 2^{8-i}, h \in \{1,2,\cdots,L-8\} \quad (6)$$

where *map* represents the map signal, which is coded with eight bits.

Step 3.6: Extract the histogram of the map to generate

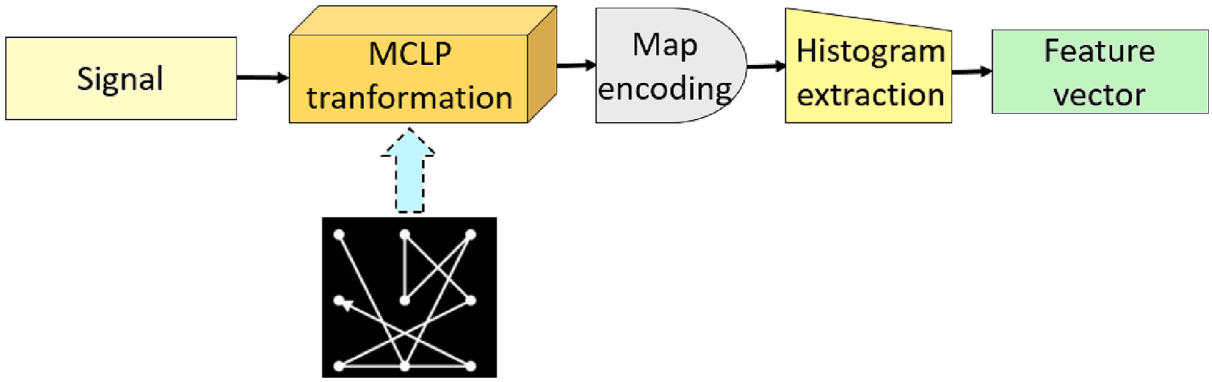

Fig. 4. Block diagram of MCLP-based feature extraction. MCLP is a directed graph used to transform each overlapping signal block (of length 9) into a map from which textural features were generated using histogram extraction.

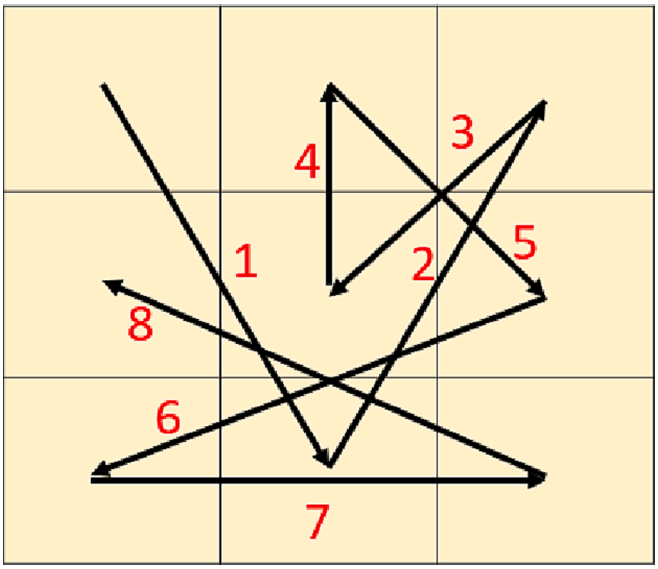

Fig. 5. Directed graph with eight directed edges (enumerated in red) used in our model. This is one of 37 unique most complicated lock patterns for a 3 × 3 matrix [36, 37]. (For interpretation of the references to colour in this figure legend, the reader is referred to the web version of this article.)

$$ft = \psi(map) \tag{7}$$

where ft represents a feature vector with length 256 (=2^8); and $\psi(.)$, histogram extraction function. Steps 3.1 to 3.6 define the MCLP feature extraction procedure.

Step 4: Concatenate the four feature vectors f^1, f^2, f^3, f^4 (each of length 2430), into a fifth feature vector of length 9720.

$$f^5 = \varpi(f^1, f^2, f^3, f^4) \tag{8}$$

where f^5 is merged feature vector and $\varpi()$ defines the feature concatenation function.

2.2.3. Multiple selector-based feature selection

Four feature selectors with unique selection attributes were used in parallel (Fig. 2). NCA and ReliefF are distance-based selectors that generate positive weights and positive plus negative weights, respectively, which are used to select the most informative features. Chi2-based selectors use the linear statistical moment, Chi2, to efficiently select the most linear features. mRMR uses information entropy and the maximum information difference to select the most valuable features. Applying these four feature selectors to the four extracted features plus the fifth merged feature vector, 20 (=4 × 5) selected feature vectors were calculated, each of which was empirically fixed at a length of 270 since our model generated 270 features from each input (raw signal or wavelet band). The steps of feature selection are detailed below.

Step 5: Apply the four feature selection methods to the five generated feature vectors to calculate 20 index vectors.

$$id^g = fs^h\left(f^k, y\right), h \in \{1,2,3,4\}, k \in \{1,2,\cdots,5\}, g \in \{1,2,\cdots,20\} \tag{9}$$

where fs^h represents the hth feature selection function; id^g, the gth sorted/qualified index.

Step 6: Choose the 270 most informative 270 features from each feature vector using the calculated sorted indexes.

$$s^g(d,r) = f^k(d, id^g(r)), d \in \{1,2,\cdots,NoS\}, r \in \{1,2,\cdots,270\} \tag{10}$$

where s represents the selected feature; and NoS, the number of signals.

2.2.4. Classification

We used a cubic SVM classifier (3rd-degree polynomial kernel) with 10-fold cross-validation to calculate one predicted vector from each of the 20 selected feature vectors.

Step 7: Classify the selected features by deploying cubic SVM.

$$p^g = SVM(s^g, y) \tag{11}$$

where p represents predicted vector; and $SVM(.)$, SVM classifier function.

2.2.5. Post-processing

We applied IHMV on the 20 predicted vectors to generate another 18 voted vectors using the mode function and a loop range of 3 to 20. After that, a greedy algorithm was applied to select the best result among all 38 vectors. The greedy algorithm is often used in optimization methods to choose the best result (Lu, Liu, Zhang, & Yin, 2022). Our model generates more than one result and the greedy algorithm has been used to select the best result.

Step 8: Generate voted vectors using the IHMV algorithm.

$$acc^g = \phi(p^g, y)$$

$$ind = argmax(acc)$$

$$v^{h-2} = \psi\left(p^{ind(1)}, p^{ind(2)}, \cdots, p^{ind(h)}\right), h \in \{3,4,\cdots,20\} \tag{12}$$

where acc represents classification accuracy; $\phi(.)$, accuracy calculation function; ind, sorted indexes per descending order of accuracy; $\psi(.)$, represents mode function; and v, voted vector. 18 (=20–3 + 1) voted vectors were generated using equation (12).

Step 9: Choose the most accurate predicted label vector by applying

the greedy algorithm.

$$acc^{g} = \phi(p^{g}, y)$$

$$acc^{g+t} = \phi(v^{t}, y), t \in \{1, 2, \cdots, 18\}$$

$$idx = argmax(acc)$$

$$fp = \begin{cases} p^{idx}, idx \leq 20 \\ v^{idx-20}, idx > 20 \end{cases} \quad (13)$$

where *idx* represents an index of the most accurate vector, and *fp* is the final predicted vector. The above nine steps define our proposed MCLP-based seismogram signal classification model.

3. Results

The parametric handcrafted feature engineering model was implemented in MATLAB (2022a) programming environment on a personal computer without needing GPU. We used the feature selectors with default settings without optimization and chose cubic SVM, which outperformed other standard classifiers in the MATLAB classification learner toolkit during preliminary testing. Standard accuracy, sensitivity, and specificity metrics were used to evaluate model performance for binary classification of earthquake versus non-earthquake (noise) seismogram signals on this balanced dataset. The mathematical notations of these parameters are given below (Powers, 2020).

$$acc = \frac{TN + TP}{TP + FN + TN + FP} \quad (14)$$

$$sen = \frac{TP}{TP + FN} \quad (15)$$

$$spe = \frac{TN}{TN + FP} \quad (16)$$

where *acc* represents accuracy; *sen*, sensitivity; *spe*, specificity; *TP*, true positives; *TN*, true negatives; *FP*, false negatives; and *FN*, false positives.

Among the 20 predicted (Numbers 1 to 20) plus 18 voted (Numbers 21 to 38) vectors, the highest accuracy, sensitivity and specificity were observed in the 25th, 17th and 22nd vectors, respectively (Table 2).

3.1. Explainable results

We were able to analyze the non-voted results of the predicted vectors according to the used signals and feature selectors. The 20 predicted vectors (Numbers 1 to 20) were read out from different combinations of signal inputs and feature selectors (the feature extraction and classifier were common to all). In comparison, the 18 voted vectors (Numbers 21 to 38) were iteratively voted using the mode function based on increasing numbers (minimum 3) of the top predicted vectors (Table 3). The best-performing non-voted predicted vector was Number 17 (Table 2), generated by combining Merged features + NCA + SVM. The best overall result was the fifth voted vector (Number 25 in Table 2), which was chosen from among the top seven most accurate predicted vectors that had been calculated based on the following combinations of signal inputs and model components: (i) Merged features + NCA + SVM, (ii) Channel X + NCA + SVM, (iii) Merged features + Chi2 + SVM, (iv) (X + Y + Z) + NCA + SVM, (v) Merged features + ReliefF + SVM, (vi) Channel X + Chi2 + SVM and (vii) Channel Y + NCA + SVM. Three out of seven models use merged features, and four use NCA feature selectors.

The most informative single channel was Channel X, which yielded 93.41% ± 3.83% accuracy, whereas the most accurate overall result of 94% ± 3.88% accuracy was attained by feeding the concatenated feature vector containing features extracted from all inputs (Fig. 6) to downstream feature selectors. The best and worst feature selectors were NCA and mRMR, which yielded general classification accuracies of 95.64% ± 0.72% and 87.95% ± 0.54%, respectively (Fig. 7).

After analyzing the relative contributions of raw input signals and their respective eight decomposed different wavelet bands (final 270 selected features), we have observed that all had contributed to the final selection, and none was redundant (Fig. 8).

The boxplots depict the corresponding minimum, first quartile, median, third quartile, and maximum values, while the blue circles show the abnormal values per the Gaussian distributions.

We have compared the relative contributions of textural versus statistical features to model prediction and observed that the former constituted the vast majority of selected features used to calculate the non-voted predicted vectors (Fig. 9). We performed ablation studies where models using only MCLP-based or statistical features were compared with our hybrid approach to investigate the contribution of statistical features. Analyzing the features extracted from channels X, Y, and Z, we observed that although statistical features alone yielded the least accurate results, their addition to the model enhanced the accuracy of MCLP-generated features considerably (Fig. 10).

4. Discussion

We have trained and tested a novel handcrafted MCLP-based XFE framework for detecting earthquake versus noise on a balanced dataset

Table 2
Performance metrics of the predicted and voted vectors.

No.	Acc (%)	Sen (%)	Spe (%)	No.	Acc (%)	Sen (%)	Spe (%)
1	95.68	94.90	96.46	20	88.24	82.98	93.50
2	95.34	94.02	96.66	21	96.86	95.86	97.86
3	94.95	94.08	95.82	22	96.58	94.78	**98.38**
4	87.68	82.76	92.60	23	96.83	95.76	97.90
5	95.34	94.52	96.16	24	96.72	95.12	98.32
6	94.79	93.38	96.20	25	**96.89**	95.80	97.98
7	94.49	93.18	95.80	26	96.71	95.20	98.22
8	87.54	82.56	92.52	27	96.75	95.52	97.98
9	94.79	94.20	95.38	28	96.68	95.16	98.20
10	94.79	93.28	96.30	29	96.75	95.50	98
11	93.93	93	94.86	30	96.65	95.14	98.16
12	87.51	82.66	92.36	31	96.71	95.44	97.98
13	95.62	94.84	96.40	32	96.56	94.96	98.16
14	92.58	89.72	95.44	33	96.53	95.08	97.98
15	94.33	93.42	95.24	34	96.45	94.74	98.16
16	88.75	83.44	94.06	35	96.42	94.90	97.94
17	96.75	**96.08**	97.42	36	96.19	94.36	98.02
18	95.63	94.20	97.06	37	96.25	94.56	97.94
19	95.37	95.18	95.56	38	96	94	98

**Acc, accuracy; Sen, sensitivity; Spe, specificity.

Table 3
Signal input and model components used to generate results.

No	Generation model	No	Generation model
1	Channel X + NCA + SVM	**20**	Merged features + mRMR + SVM
2	Channel X + Chi2 + SVM	**21**	Top 3 predicted vectors
3	Channel X + ReliefF + SVM	**22**	Top 4 predicted vectors
4	Channel X + mRMR + SVM	**23**	Top 5 predicted vectors
5	Channel Y + NCA + SVM	**24**	Top 6 predicted vectors
6	Channel Y + Chi2 + SVM	**25**	Top 7 predicted vectors
7	Channel Y + ReliefF + SVM	**26**	Top 8 predicted vectors
8	Channel Y + mRMR + SVM	**27**	Top 9 predicted vectors
9	Channel Z + NCA + SVM	**28**	Top 10 predicted vectors
10	Channel Z + Chi2 + SVM	**29**	Top 11 predicted vectors
11	Channel Z + ReliefF + SVM	**30**	Top 12 predicted vectors
12	Channel Z + mRMR + SVM	**31**	Top 13 predicted vectors
13	(X + Y + Z) + NCA + SVM	**32**	Top 14 predicted vectors
14	(X + Y + Z) + Chi2 + SVM	**33**	Top 15 predicted vectors
15	(X + Y + Z) + ReliefF + SVM	**34**	Top 16 predicted vectors
16	(X + Y + Z) + mRMR + SVM	**35**	Top 17 predicted vectors
17	Merged features + NCA + SVM	**36**	Top 18 predicted vectors
18	Merged features + Chi2 + SVM	**37**	Top 19 predicted vectors
19	Merged features + ReliefF + SVM	**38**	All predicted vectors

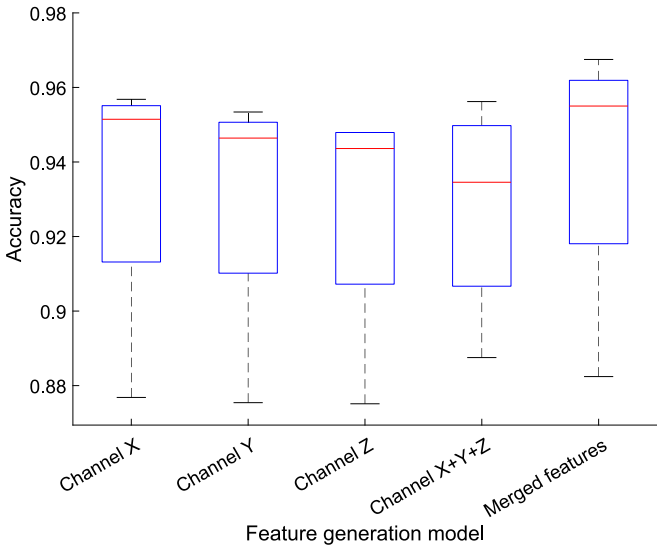

Fig. 6. Accuracies attained using various feature vectors.

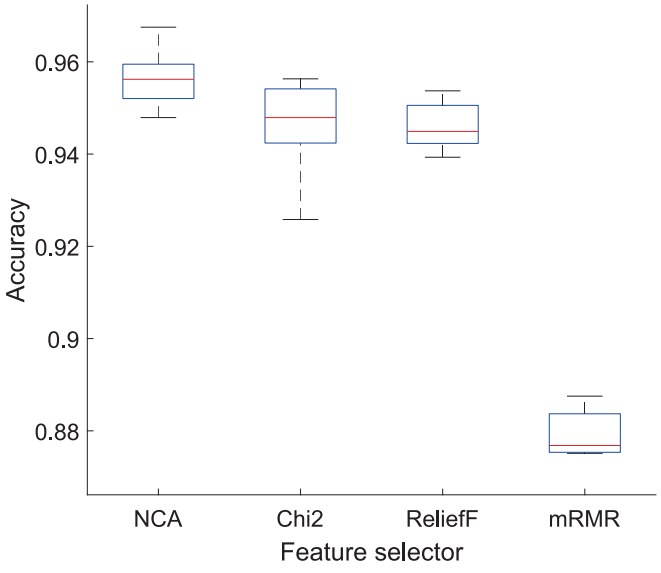

Fig. 7. Accuracies attained using different feature selectors.

that had been modified from a public seismogram signal database. The model is the first XAI model for earthquake detection, which facilitated the identification of the optimal model components: the most informative single channel, feature extraction method, and feature selector were Channel X, MCLP-generated textural features, and NCA, respectively. As a result, our model attained excellent 96.75% and 96.89% classification accuracies using non-voted and voted vectors, respectively.

In the classification phase, we used a cubic SVM classifier, which had been chosen after testing standard classifiers organized into eight categories and various SVM subtypes on the MATLAB classification learner toolkit. As a result, SVM outperformed the other classifiers (Fig. 11A), and cubic SVM was evaluated to be the most accurate SVM subtype (Fig. 11B).

4.1. Comparison with the literature

Our handcrafted and computationally lightweight XFE model delivered classification performance commensurate with recently published deep models (Kong et al., 2021; Magrini et al., 2020; Majstorović et al., 2021) (Table 4). The other models used convolutional neural

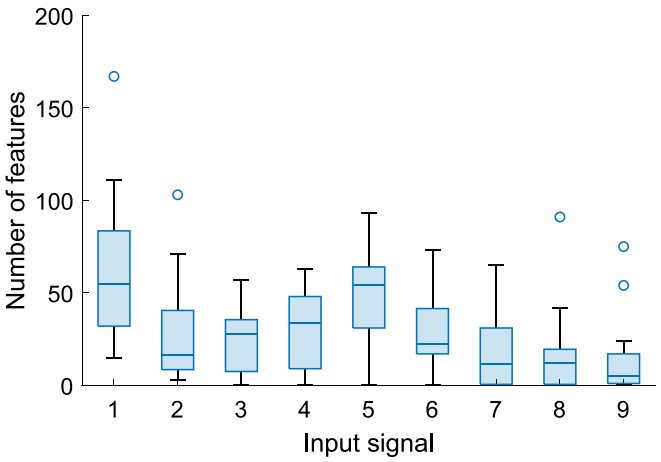

Fig. 8. Frequency distribution of selected features extracted from raw input signals (1) and the different wavelet bands (2 to 9) that contributed to the 20 non-voted results.

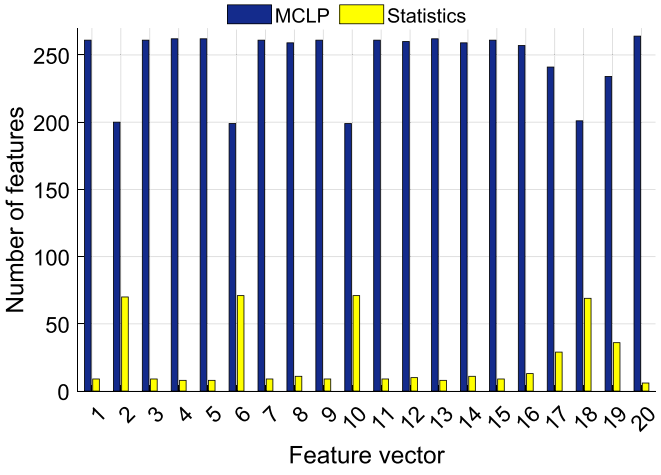

Fig. 9. Frequency distribution of textural and statistical features among the 20 selected feature vectors.

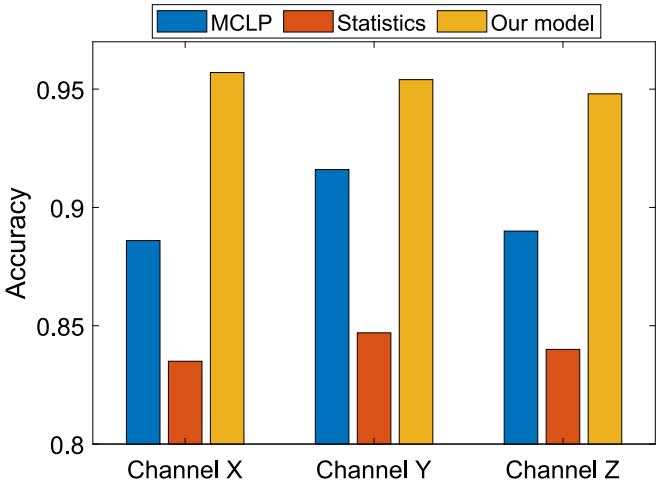

Fig. 10. Classification accuracies of MCLP-based textural and statistical feature ablation models compared with our hybrid textural and feature extraction model.

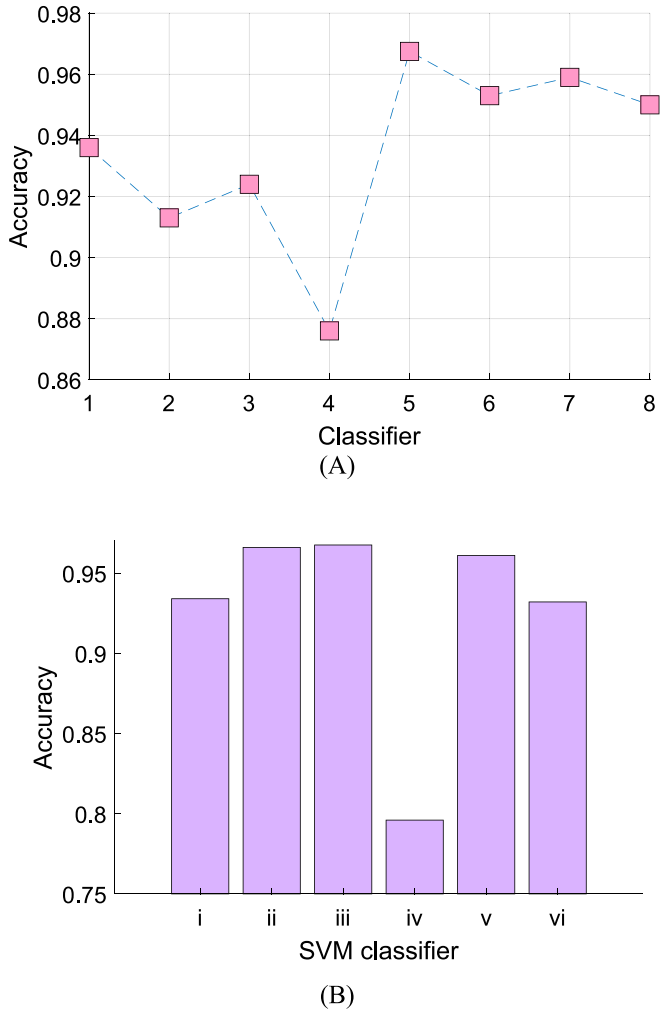

Fig. 11. Evaluation of eight categories of classifiers (A) and six SVM subtypes (B) on MATLAB classification learner toolkit using the optimal selected feature vector obtained by inputting the merged feature vector to NCA selector. The classifier categories are decision tree (1), discriminant (2), linear regression (3), naïve Bayes (4), SVM (5), k-nearest neighbor (6), ensemble (7), and neural network (8); and the SVM subtypes are linear (i), quadratic (ii), cubic (iii), fine Gaussian (iv), medium Gaussian (v), and coarse Gaussian (vi).

networks (CNNs), which are inherently computationally complex. While Meier et al. (Meier et al., 2019) attained the highest precision and recall values, adding a generative adversarial network to CNN considerably compounded the model's computation cost. Authors in (Kong et al., 2021; Magrini et al., 2020; Majstorović et al., 2021) have employed holdout validations, we used 10-fold cross-validation to develop the model. Our results were obtained using the smallest dataset, a subset of the Len-DB database [18]; our model outperformed other models developed on the full Len-DB database [18, 20].

As shown in Table 4, the studies in the literature used deep learning models such as CNN. Although CNN-based methods produce high classification results, the time cost is relatively high in these methods. On the other hand, our proposed MCLP-based framework is a lightweight method. Therefore, its time complexity is considerably lower than CNN. In addition, CNN-based methods have many layers, making the structure complex. But our method consists of classical machine learning steps: feature extraction, feature selection, and classification. Hence, we obtained good results using a simple, less complex model.

Table 4
Comparison of our model with published earthquake detection models.

Paper	Method	Dataset	Validation	Results
Meier 2019 (Meier et al., 2019**)**	CNN, generative adversarial network, random forest classifier	Combined dataset	Holdout CV (80:20)	Pre 99.5% Rec 99.3%
Magrini 2020 (Magrini et al., 2020**)**	Custom designed CNN	Len-DB	Holdout CV (71:21.5:7.5)	Acc 93.2%
Majstorović 2021 (Majstorović et al., 2021**)**	Custom designed CNN	Own dataset	Holdout CV (80:10:10)	Acc 97.0%
Kong 2021 (Kong et al., 2021**)**	Autoencoder-based feature extraction, CNN	Len-DB	Holdout CV (46:14:30)	Acc 90%
Our method	TQWT signal decomposition, MCLP and statistical feature extraction, multiple feature selectors, SVM, IHMV	Subset of Len-DB	10-fold CV	Acc 96.89% Sen 96.08% Spe 98.38%

**CNN: convolutional neural network; CV: cross-validation.

4.2. Highlights and limitations

We used MCLP to extract textural features from seismogram signals for earthquake detection. Our approach included multilevel hybrid statistical and MCLP-based feature extraction, feature vector concatenation, multiple feature selectors, a shallow SVM classifier, and IHMV for result selection. Unlike "black box" deep learning models, the contributions of the various signal inputs to and model components in our parametric architecture were readily analyzable. From such analyses, we observed that while the most discriminative individual channel was Channel X, superior results were obtained by merging the signals of all three channels and merging the feature extraction readouts of the individual and merged channels. Moreover, MCLP-generated textural features, the merging of feature vectors, and the NCA selector were demonstrated to be the most valuable features, feature generation method and feature selector, respectively. Hence, our model can be considered the first automated seismogram-based XAI model for earthquake detection. Additionally, the model became fully self-organized using the greedy algorithm and IHMV method. Our model attained good classification performance commensurate with the literature at a linear computational cost.

We used default classifier settings without hyperparameter optimization, which potentially could have improved classification performance. We empirically elected to choose the most informative 270 features across all four feature selectors. To improve classification performance, iterative versions of these selectors could have been deployed to calculate the selector-specific optimal numbers of the most discriminative features, but at the cost of multiplied time complexity burdens depending on the number of iterative runs.

5. Conclusion

Our earthquake detection model employed a novel XFE model using TQWT-based signal decomposition, hybrid statistical features, MCLP-based textural feature extraction, feature vector merging, multiple feature selectors, SVM classifier, IHMV, and a greedy algorithm for result selection. The model attained good binary earthquake versus non-earthquake signal classification on a public three-channel seismogram dataset commensurate with deep models but at a lower computational cost. Moreover, we have presented detailed classification results stratified by individual and merged channel signal inputs, raw input and decomposed wavelet bands, textural versus statistical features,

individual and merged features vectors, and individual feature selectors. We demonstrated that MCLP-generated textural features (Fig. 9), merging of feature vectors (Fig. 6), and NCA selector (Fig. 7) contributed the most to predicted vector accuracy. Moreover, ablation studies demonstrated the statistical features added to MCLP-generated features enhanced the model accuracy considerably (Fig. 10). Unlike deep models that require tuning of millions of parameters, our handcrafted XFE model possesses linear time complexity and is computationally lightweight, which should enhance its ease of implementation and adoption among interested researchers/developers.

Funding

This research is supported by the South African National Library and Information Consortium (SANLiC).

CRediT authorship contribution statement

Suat Gokhan Ozkaya: Conceptualization, Methodology, Software, Validation, Formal analysis, Investigation, Resources, Data curation, Writing – original draft, Writing – review & editing, Visualization. **Nursena Baygin:** Conceptualization, Methodology, Validation, Formal analysis, Investigation, Resources, Data curation, Writing – original draft, Writing – review & editing, Visualization. **Prabal D. Barua:** Conceptualization, Methodology, Validation, Formal analysis, Investigation, Resources, Data curation, Writing – original draft, Writing – review & editing, Visualization. **Arvind R. Singh:** Conceptualization, Methodology, Validation, Formal analysis, Investigation, Resources, Data curation, Writing – original draft, Writing – review & editing, Visualization, Funding acquisition. **Mohit Bajaj:** Conceptualization, Methodology, Validation, Formal analysis, Investigation, Resources, Data curation, Writing – original draft, Writing – review & editing, Visualization. **Mehmet Baygin:** Conceptualization, Methodology, Validation, Formal analysis, Resources, Data curation, Writing – original draft, Writing – review & editing. **Sengul Dogan:** Conceptualization, Methodology, Validation, Resources, Data curation, Writing – original draft, Writing – review & editing. **Turker Tuncer:** Conceptualization, Methodology, Software, Validation, Resources, Data curation, Writing – original draft, Writing – review & editing. **Ru-San Tan:** Conceptualization, Methodology, Validation, Resources, Writing – original draft, Writing – review & editing. **U. Rajendra Acharya:** Conceptualization, Methodology, Validation, Resources, Writing – original draft, Writing – review & editing, Supervision, Project administration.

Declaration of Competing Interest

The authors declare that they have no known competing financial interests or personal relationships that could have appeared to influence the work reported in this paper.

Data availability

The authors do not have permission to share data.

References

An, J., Tao, L., Jiang, L., Yan, H., 2021. A shaking table-based experimental study of seismic response of shield-enlarge-dig type's underground subway station in liquefiable ground. Soil Dyn. Earthq. Eng. 147, 106621.

Bolton, D.C., Shreedharan, S., Rivière, J., Marone, C., 2020. Acoustic energy release during the laboratory seismic cycle: insights on laboratory earthquake precursors and prediction. J. Geophys. Res. Solid Earth 125 (8) e2019JB018975.

Dogan, A., Akay, M., Barua, P.D., Baygin, M., Dogan, S., Tuncer, T., Dogru, A.H., Acharya, U.R., 2021. PrimePatNet87: Prime pattern and tunable q-factor wavelet transform techniques for automated accurate EEG emotion recognition. Comput. Biol. Med. 138, 104867.

Eftekhari, A., Samadzadegan, F., Dadrass Javan, F., 2023. Building change detection using the parallel spatial-channel attention block and edge-guided deep network. Int. J. Appl. Earth Obs. Geoinf. 117, 103180.

Ghanbari, H., Antoniades, D., 2022. Convolutional neural networks for mapping of lake sediment core particle size using hyperspectral imaging. Int. J. Appl. Earth Obs. Geoinf. 112, 102906.

Goldberger, J., Hinton, G.E., Roweis, S., Salakhutdinov, R.R., 2004. Neighbourhood components analysis. Adv. Neural Inf. Proces. Syst. 17, 513–520.

Hafner, K., Clayton, R.W., 2001. The Southern California Earthquake Data Center (SCEDC). Seismol. Res. Lett. 72 (6), 705–711.

Jozinović, D., Lomax, A., Štajduhar, I., Michelini, A., 2020. Rapid prediction of earthquake ground shaking intensity using raw waveform data and a convolutional neural network. Geophys. J. Int. 222 (2), 1379–1389.

Kavianpour, P., Kavianpour, M., Jahani, E., & Ramezani, A. (2021). *Earthquake Magnitude Prediction using Spatia-temporal Features Learning Based on Hybrid CNN-BiLSTM Model.* Paper presented at the 2021 7th International Conference on Signal Processing and Intelligent Systems (ICSPIS).

Kong, Q., Chiang, A., Aguiar, A.C., Fernández-Godino, M.G., Myers, S.C., Lucas, D.D., 2021. Deep convolutional autoencoders as generic feature extractors in seismological applications. Artificial Intelligence in Geosciences 2, 96–106.

Kuncan, F., Yılmaz, K., Kuncan, M., 2019. Sensör işaretlerinden cinsiyet tanıma için yerel ikili örüntüler tabanlı yeni yaklaşımlar. Gazi Üniversitesi Mühendislik Mimarlık Fakültesi Dergisi 34 (4), 2173–2186.

Li, W., Chakraborty, M., Sha, Y.u., Zhou, K., Faber, J., Rümpker, G., Stöcker, H., Srivastava, N., 2022. A study on small magnitude seismic phase identification using 1D deep residual neural network. Artificial Intelligence in Geosciences 3, 115–122.

Li, Z., Meier, M.A., Hauksson, E., Zhan, Z., Andrews, J., 2018. Machine learning seismic wave discrimination: Application to earthquake early warning. Geophys. Res. Lett. 45 (10), 4773–4779.

Liu, H., & Setiono, R. (1995). *Chi2: Feature selection and discretization of numeric attributes.* Paper presented at the Proceedings of 7th IEEE International Conference on Tools with Artificial Intelligence.

Loh, H.W., Ooi, C.P., Seoni, S., Barua, P.D., Molinari, F., Acharya, U.R., 2022. Application of explainable artificial intelligence for healthcare: A systematic review of the last decade (2011–2022). Comput. Methods Programs Biomed. 226, 107161.

Lu, C., Liu, Q., Zhang, B., Yin, L., 2022. A Pareto-based hybrid iterated greedy algorithm for energy-efficient scheduling of distributed hybrid flowshop. Expert Syst. Appl. 204, 117555.

Lv, L., Chen, T., Dou, J., Plaza, A., 2022. A hybrid ensemble-based deep-learning framework for landslide susceptibility mapping. Int. J. Appl. Earth Obs. Geoinf. 108, 102713.

Magrini, F., Jozinović, D., Cammarano, F., Michelini, A., Boschi, L., 2020. Local earthquakes detection: A benchmark dataset of 3-component seismograms built on a global scale. Artif. Intell. Geosci. 1, 1–10.

Majstorović, J., Giffard-Roisin, S., Poli, P., 2021. Designing convolutional neural network pipeline for near-fault earthquake catalog extension using single-station waveforms. J. Geophys. Res. Solid Earth 126 (7) e2020JB021566.

Malfante, M., Dalla Mura, M., Métaxian, J.-P., Mars, J.I., Macedo, O., Inza, A., 2018. Machine learning for volcano-seismic signals: Challenges and perspectives. IEEE Signal Process Mag. 35 (2), 20–30.

Mandal, S., Maiti, R. (Eds.), 2015. Semi-quantitative Approaches for Landslide Assessment and Prediction. Springer Singapore, Singapore.

Meier, M.-A., Ross, Z.E., Ramachandran, A., Balakrishna, A., Nair, S., Kundzicz, P., Li, Z., Andrews, J., Hauksson, E., Yue, Y., 2019. Reliable real-time seismic signal/noise discrimination with machine learning. J. Geophys. Res. Solid Earth 124 (1), 788–800.

Mousavi, S.M., Beroza, G.C., 2020. A machine-learning approach for earthquake magnitude estimation. Geophys. Res. Lett. 47 (1) e2019GL085976.

Mousavi, S.M., Sheng, Y., Zhu, W., Beroza, G.C., 2019. STanford EArthquake Dataset (STEAD): A global data set of seismic signals for AI. IEEE Access 7, 179464–179476.

Otović, E., Njirjak, M., Jozinović, D., Mauša, G., Michelini, A., Štajduhar, I., 2022. Intra-domain and cross-domain transfer learning for time series data—How transferable are the features? Knowl.-Based Syst. 239, 107976.

Pavel, F., 2021. Analysis of pulse-like ground motion recordings from Vrancea intermediate-depth earthquakes. J. Seismol. 25 (2), 733–745.

Powers, D. M. (2020). Evaluation: from precision, recall and F-measure to ROC, informedness, markedness and correlation. *arXiv preprint arXiv:2010.16061*.

Qing, Y., Ming, D., Wen, Q.i., Weng, Q., Xu, L.u., Chen, Y., Zhang, Y.i., Zeng, B., 2022. Operational earthquake-induced building damage assessment using CNN-based direct remote sensing change detection on superpixel level. Int. J. Appl. Earth Obs. Geoinf. 112, 102899.

Radovic, M., Ghalwash, M., Filipovic, N., Obradovic, Z., 2017. Minimum redundancy maximum relevance feature selection approach for temporal gene expression data. BMC Bioinf. 18 (1), 1–14.

Robnik-Šikonja, M., Kononenko, I., 2003. Theoretical and empirical analysis of ReliefF and RReliefF. Mach. Learn. 53 (1), 23–69.

Rost, S., Earle, P.S., Shearer, P.M., Frost, D.A., Selby, N.D., 2015. Seismic detections of small-scale heterogeneities in the deep Earth. In: The Earth's Heterogeneous Mantle. Springer, pp. 367–390.

Saad, O.M., Chen, Y., Savvaidis, A., Chen, W., Zhang, F., Chen, Y., 2022. Unsupervised deep learning for single-channel earthquake data denoising and its applications in event detection and fully automatic location. IEEE Trans. Geosci. Remote Sens. 60, 1–10.

Saraf, A.K., Rawat, V., Choudhury, S., Dasgupta, S., Das, J., 2009. Advances in understanding of the mechanism for generation of earthquake thermal precursors detected by satellites. Int. J. Appl. Earth Obs. Geoinf. 11 (6), 373–379.

Selesnick, I.W., 2011. Wavelet transform with tunable Q-factor. IEEE Trans. Signal Process. 59 (8), 3560–3575.

Tasci, G., Loh, H.W., Barua, P.D., Baygin, M., Tasci, B., Dogan, S., Tuncer, T., Palmer, E. E., Tan, R.-S., Acharya, U.R., 2023. Automated accurate detection of depression using twin Pascal's triangles lattice pattern with EEG Signals. Knowl.-Based Syst. 260, 110190.
van der Meijde, M., Pail, R., Bingham, R., Floberghagen, R., 2015. GOCE data, models, and applications: A review. Int. J. Appl. Earth Obs. Geoinf. 35, 4–15.
Vapnik, V., 1998. The support vector method of function estimation. In: Nonlinear Modeling. Springer, pp. 55–85.
Wald, D.J., 2020. Practical limitations of earthquake early warning. Earthq. Spectra 36 (3), 1412–1447.
Wang, T., DeGrandpre, K., Lu, Z., Freymueller, J.T., 2018. Complex surface deformation of Akutan volcano, Alaska revealed from InSAR time series. Int. J. Appl. Earth Obs. Geoinf. 64, 171–180.
Wei, R., Ye, C., Sui, T., Ge, Y., Li, Y., Li, J., 2022. Combining spatial response features and machine learning classifiers for landslide susceptibility mapping. Int. J. Appl. Earth Obs. Geoinf. 107, 102681.
Xiu, H., Liu, X., Wang, W., Kim, K.-S., Shinohara, T., Chang, Q., Matsuoka, M., 2023. DS-Net: A dedicated approach for collapsed building detection from post-event airborne point clouds. Int. J. Appl. Earth Obs. Geoinf. 116, 103150.
Zhu, W., Tai, K.S., Mousavi, S.M., Bailis, P., Beroza, G.C., 2022. An End-To-End Earthquake Detection Method for Joint Phase Picking and Association Using Deep Learning. J. Geophys. Res. Solid Earth 127 (3) e2021JB023283.
Zye, D. (2021). MCLP, Retrieved from https://summerofmathexposition.substack.com/.